*Manuscript
Click here to view linked References

Complex Transition Metal Hydrides Incorporating Ionic Hydrogen: Synthesis and Characterization of $Na_2Mg_2FeH_8$ and $Na_2Mg_2RuH_8$

Terry D. Humphries [a]*, Shigeyuki Takagi [b], Guanqiao Li [b], Motoaki Matsuo [b], Toyoto Sato [b], Magnus H. Sørby [c], Stefano Deledda [c], Bjørn C. Hauback [c], Shin-ichi Orimo [a,b]

[a] WPI-Advanced Institute for Materials Research, Tohoku University, Sendai 980-8577, Japan

[b] Institute for Materials Research, Tohoku University, Sendai 980-8577, Japan

[c] Physics Department, Institute for Energy Technology, Kjeller NO-2027, Norway

Corresponding Author. Tel: +81-22-215-2094; Fax: +81-22-215-2091; E-mail: terry_humphries81@hotmail.com

Abstract

A new class of quaternary complex transition metal hydrides ($Na_2Mg_2TH_8$ (T = Fe, Ru)) have been synthesized and their structures determined by combined synchrotron radiation X-ray and powder neutron diffraction. The compounds can be considered as a link between ionic and complex hydrides in terms of incorporating independently coordinated ionic and covalent hydrogen. These novel isostructural complex transition metal hydrides crystallize in the

orthorhombic space group *Pbam*, where the octahedral complex hydride anion is surrounded by a cubic array of four Mg^{2+} and four Na^{+} cations, forming distinct two-dimensional layers. An intriguing feature of these materials is the distorted octahedral coordination of the isolated H^{-} anions by four Na^{+} and two Mg^{2+} cations, which form layers between the transition metal containing layers. The vibrational modes of the H^{-} anions and complex hydride anion are independently observed for the first time in a quaternary complex transition metal hydride system by Raman and IR spectroscopy.

Keywords: metal hydrides; mechanochemical processing; crystal structure; neutron diffraction; X-ray diffraction; energy storage materials.

1. Introduction

Homoleptic complex transition metal hydrides are extremely versatile, have a rich and varied chemistry and as such exist in a variety of structural conformations [1]. Since the first report of Mg_2NiH_4 in 1968 [2], a diverse selection of complex transition metal hydride anions have been synthesized with transition metals ranging from group 7 to 12. The complex hydride anion is electronically stabilized by the positive charge of the polarizable alkali, alkali-earth, or lanthanide elements, which form cubic arrays around the anion. Until recently it was assumed that it was only possible to synthesize $[NiH_4]^{4-}$ or $[FeH_6]^{4-}$ complexes (in quantitative yields) with divalent or trivalent cations (Mg, Yb, Sr, Ba, Ca, La) [3–5], however, the alkali metal containing $YLiFeH_6$ [6], Li_4FeH_6 [7] and $Na_2Mg_2NiH_6$ ($2Na^{+}\cdot 2Mg^{2+}\cdot[NiH_4]^{4-}\cdot 2H^{-}$) [8,9], were recently reported.

Complex transition metal hydrides have long been of interest as potential hydrogen storage materials [10] and it has been identified that the hydrogen capacity and thermodynamics of these materials can be tuned by varying the cations [3,11,12]. As such, first-principles calculations have determined that increasing the electronegativity of the cation decreases the thermal stability of the hydride [11]. Other studies have also determined distinct correlations involving the physical properties of the cation or "cation matrix effects" on the vibrational stretching modes of the complex hydride [13].

It was recently proposed that increasing the total anionic charge of the system with isolated anionic hydrogen allows for the inclusion of a wider variety of cations into the system and therefore the formation of compounds that were once considered not possible to synthesize [12]. With these concepts in mind, first-principles DFT calculations have been performed on a variety of hypothetical quaternary complex transition metal hydrides with incorporation of H^- to determine their feasibility to be synthesized [12]. Based on this these calculations, $Na_2Mg_2TH_8$ ($2Na^+ \cdot 2Mg^{2+} \cdot [TH_6]^{4-} \cdot 2H^-$) ($T$ = Fe, Ru) have been successfully synthesized and their structures determined by combined synchrotron radiation powder X-ray diffraction (SR-PXD) and powder neutron diffraction (PND). Here we present a detailed description of the crystal structures suggested by DFT and refined by the Rietveld method for $Na_2Mg_2FeH_8$ and $Na_2Mg_2RuH_8$, with an emphasis on the diversity of metal to hydrogen bonds displayed by these species. This structural study based on diffraction data is supported by Raman and FT-IR spectroscopies and corroborated by DFT calculations, where the vibrational modes of the anionic hydrogen and complex hydride anion are independently observed for the first time in a quaternary transition metal hydride.

2. Materials and Methods

All preparation and manipulation was performed in a Miwa glove box filled with purified argon (less than 1 ppm O_2 and the dew point of H_2O below 190 K) to avoid contamination.

2.1 Synthesis of $Na_2Mg_2FeH(D)_8$. The synthesis of $Na_2Mg_2FeH_8$ followed a four step process, which first required the synthesis of Mg_2FeH_6. This was achieved by mechanically milling (Fritsch Pulverisette 7) MgH_2 (hydrogen storage grade, Sigma Aldrich) and Fe (99.99%, Mitsuwa) powders at a molar ratio of 2:1 for 2 h at 400 rpm (ball-to-powder ratio 40:1), under argon with subsequent heat treatment at 400 °C for 20 h under 3 MPa H_2. The resultant olive green powder was then mechanically milled with NaH (95 %, Sigma Aldrich) at a molar ratio of 1:2 for 20 h under argon with subsequent heat treatment at 400 °C for 20 h under 30 MPa H_2. The product was yielded as an olive green powder. The deuteride analogue was synthesized using identical starting materials (MgH_2, NaH and Fe), albeit using D_2 gas instead of H_2.

2.2 Synthesis of $Na_2Mg_2RuH(D)_8$. The synthesis of $Na_2Mg_2RuH_8$ followed a two-step process. MgH_2, NaH and Ru (99.9 %, Kojundo Chemical Laboratory) were mechanically milled (identical parameters as employed with $Na_2Mg_2FeH_8$) at a molar ratio of 2:2:1 for 20 h under argon, before subsequent heat treatment at 500 °C for 20 h under 30 MPa H_2. The product was yielded as a light grey powder. The deuteride analogue was synthesized using identical starting materials (MgH_2, NaH and Ru), albeit using D_2 gas instead of H_2.

2.3 Synchrotron radiation powder X-ray diffraction (SR-PXD). Measurements were performed using the Swiss-Norwegian Beamline (SNBL, BM01A) at the European Synchrotron Radiation Facility (ESRF) in Grenoble, France. The sample was loaded inside a sealed boron glass capillary (0.5 mm inner diameter). A two-dimensional SR-PXD pattern (λ = 0.70135 Å) was collected using a fast pixel detector (Pilatus 2M, Dectris) with an exposure time of 30 sec,

with a sample to detector distance of 143 mm. The capillary was rotated 30° during exposure to improve the powder averaging. The data were integrated to one-dimensional diffraction patterns with the program Fit2D [14]. Calibration was performed using a NIST LaB_6 standard.

2.4 Powder neutron diffraction (PND). Data were collected with the PUS instrument at the JEEP II reactor in Kjeller, Norway [15]. Neutrons with the wavelength $\lambda = 1.5548$ Å were obtained from a Ge (5 1 1) vertically focusing monochromator. Data were collected from 10° to 130° in 2θ and binned with $\Delta 2\theta = 0.05°$. The sample was mounted in the glove box and contained in a rotating cylindrical vanadium sample holder with 6 mm inner diameter, and then sealed with an indium wire to prevent air exposure.

2.5 Structure Determination. The structural model used for refinement was initially calculated and optimized by first principle methods [12] and the lattice parameters checked against data measured at room temperature using DICVOL06 [16] and CHEKCELL [17]. The combined structural refinements using SR-PXD and PND data of $Na_2Mg_2FeD_8$ and $Na_2Mg_2RuD_8$ with the Rietveld method were performed using the GSAS software package [18], with the graphical interface EXPGUI [19]. For the Rietveld refinements the *T*−D (*T* = Fe, Ru) and *M*−D2 (*M* = Na, Mg) bond distances were initially restrained to those calculated by DFT calculations (see Supplementary Information), while D1−D3 bond distances were restrained to 2.2 Å. All restraints were then removed to obtain convergence, thus allowing free refinement of all atomic coordinates. Isotropic displacement parameters, U_{iso}, were refined as a single parameter for the two covalently bonded H atoms. All backgrounds were modelled by a Shifted Chebyschev polynomial; for $Na_2Mg_2FeD_8$ this consisted of 36 points, while the backgrounds for $Na_2Mg_2RuD_8$ were modelled by 36 (SR-XRD) and 16 (PND) manually placed points. A Thomson-Cox-Hastings pseudo-Voigt profile function was selected for the global refinement of

the SR-PXD and PND data sets. Unit cell parameters, zero-point, overall scale factors, peak shape mixing parameters, three Gaussian profile parameters (U,V,W), and two Lorentzian profile parameters (X, Y) were refined for each data set. Within the $Na_2Mg_2RuD_8$ powder, one unknown phase was identified, which was indexed according to a tetragonal unit cell (see Supplementary Information). Due to the small fraction of this phase, structure solution was not possible, and as such was refined by the Le Bail method simultaneously to the refinement of the known phases by the Rietveld method.

2.6 Vibrational Spectroscopy. FT-IR measurements were conducted using a Thermo Nicolet IN10 infrared microscope. A few granules of the hydride were inserted into a diamond sample accessory and spectra were collected in transmission mode. The powders were measured at the same position after releasing pressure to guarantee the sample was not affected by pressure. Measurements were conducted over the spectral range of 4000 – 400 cm^{-1} for 3600 scans, at a resolution of 8 cm^{-1}. Raman spectroscopy measurements were conducted using a Thermo Nicolet Almega-HD Raman Microscope over the spectral range of 98 to 3703 cm^{-1} using a semiconductor laser operating at 512 nm at 20 % power. Samples were measured at room temperature as compressed pellets (12 MPa) placed inside an inert atmosphere container with a quartz lid and measured for 0.5 s per scan for a total of 2000 scans. An aperture size of 100 μm was used. Assignment of the features in both the Raman and FT-IR spectra was assisted using vibrational frequencies generated from the DFT calculations and identified by reference to the displacement vectors for each of the vibrations.

2.7 DFT phonon calculations. Γ-point phonon calculations for the 26-atom primitive unit cell of $Na_2Mg_2FeH_8$ were performed using a plane-wave basis and projector augmented wave method [20,21] within the generalized gradient approximation of Perdew, Burke, and Ernzerhof (PBE)

[22], as implemented in the Vienna Ab-Initio Simulation Package (VASP) [23,24]. Well-converged plane-wave basis sets were employed with cutoff energies of 600 and 5400 eV for the wavefunction and charge density, respectively. A 6×6×2 grid was used for the ***k***-point sampling of the Brillouin zone.

3. Results and Discussion

3.1 Phase Identification

The SR-PXD and PND patterns measured for $Na_2Mg_2FeD_8$ and $Na_2Mg_2RuD_8$ are illustrated in Fig. 1. The dominant set of Bragg peaks observed for both $Na_2Mg_2FeD_8$ and $Na_2Mg_2RuD_8$ were indexed to a primitive orthorhombic unit cell with dimensions a = 5.30527(8), b = 11.03743(16) and c = 4.47783(6) Å; and a = 5.37969(5), b = 11.11847(10) and c = 4.64792(4) Å, respectively and extinction rules according to the space group *Pbam*. The crystallographic information for both compounds and their atomic positions are tabulated in Table 1, while the crystal structure is illustrated in Fig. 2a. The initial structure models were derived from total energy calculations based on DFT [12], while the combination of the SR-PXD and PND data on the structure model were used in the Rietveld refinements. For $Na_2Mg_2FeD_8$, this resulted in the following reliability factors: R_{wp} = 0.080 for the SR-PXD pattern and R_{wp} = 0.067 for the PND data set. For $Na_2Mg_2RuD_8$ this resulted in the following reliability factors: R_{wp} = 0.055 for the SR-PXD pattern and R_{wp} = 0.055 for the PND data set. The relatively high baseline of the PND data for $Na_2Mg_2RuD_8$ compared to $Na_2Mg_2FeD_8$ (Figs. 2b and 2d) is due to lower data statistics caused by a shortened period of data collection.

FIGURE 1

Table 1.

FIGURE 2

Phase composition analysis by Rietveld refinement of the SR-PXD data determined that $Na_2Mg_2FeD_8$ has been synthesized to 87.0(3) % purity, along with 5.66(4) % Fe, 4.06(4) % Mg_2FeD_6, and 3.27(6) % NaD (Fig. 1a). This suggests that the reaction may not have gone to completion, even though the sample was annealed under a D_2 environment of 30 MPa for 60 h. $Na_2Mg_2RuD_8$ has been synthesized to 96.77(4) % purity, with 3.23(3) % Ru starting material remaining (Fig. 1c). NaD was not observed. An unknown material was also identified within the $Na_2Mg_2RuD_8$ powder, of which a few reflections were discernable. These Bragg peaks were indexed to a possible tetragonal unit cell with dimensions a = 8.9150(4) Å and c = 5.2442(4) Å. Unfortunately, the low levels of the material inhibited structural determination, while in addition it was not possible to identify the structure against the ICSD database (the d spacing of the observed peaks in the SR-PXD data are listed in the Supplementary Information). Using the program CHEKCELL [17], a space group of *P*42*nm* was adjudged, which was subsequently used to fit the data using the Le Bail method in GSAS. The total fraction of the unknown material in the powder was evaluated as 0.7 wt%.

3.2 Structure of $Na_2Mg_2TD_8$ (T = Fe, Ru)

In $Na_2Mg_2FeD_8$, the Fe, D1 and D3 atoms are bonded in an octahedral arrangement, with the two axial Fe−D1 bonds having a bond distance of 1.610(9) Å and the four equatorial Fe−D3 bonds at a distance of 1.592(6) Å (Fig. 2b and Table 2). The refined Fe−D bond lengths are in good agreement with the DFT calculated values (Supplementary Information) and with other $[FeD_6]^{4-}$ complexes (e.g. Mg_2FeD_6 = 1.5561(2) Å [25]; Ca_2FeD_6 = 1.6176(2) Å [4]), and are also

in trend with analogous $[TD_x]^{4-}$ (T = Ni, Ru, Co, Os) complexes (which vary according to the atomic radii of T) [3,4,9,25–27]. While the D1 and D3 atoms form covalent bonds with T and are also coordinated by Mg^{2+} and Na^{+}, the D2 atoms form ionic bonds to only four Na^{+} and two Mg^{2+} (Fig. 2c). The Na−D2 bond distances of 2.585(6) Å are similar to that of the archetypical ionic NaD of 2.445 Å [28].

Table 2.

Each $[FeD_6]^{4-}$ octahedron is surrounded by a distorted cube consisting of four Na^{+} and four Mg^{2+} (Fig. 2b), similar to that observed in the archetypical Mg_2TD_6 (T = Fe, Ru) and related compounds [3,4,9,25,29,30]. The D1 atoms are bonded to two Na^{+} at distances of 2.484(10) and 2.822 (10) Å and two Mg^{2+} (2.2457(7) Å), while the D3 atoms are also connected with two Mg (2.118(7) and 2.139(7) Å) and two Na atoms (2.373(7) and 2.551(7) Å). The elongation of the Fe−D1 and M−D1 (M = Na, Mg) bond distances, compared to the corresponding D3 bond distances, is due to the additional coordination of D1 by a Na^{+} belonging to the neighboring cube in the *b*-direction (Fig. 2d). This arises as the Fe, D1 and Na atoms are aligned on the edges of the unit cell occupying the 2*a* (Fe) and 4*g* (D1 and Na) sites creating a Fe−D1−Na bond angle of 168.5(6)°, with a D1−Na bond distance of 2.382(9) Å.

Looking closer at the crystal packing of $Na_2Mg_2FeD_8$, the cubes containing $[FeD_6]^{4-}$ are connected in an edge-sharing two-dimensional network forming layers along the *a*/*c* plane, with a sheet of D2 atoms (D^{-}) occupying the 4*h* sites in between (Fig. 2a). This edge-sharing packing is analogous to that observed in the quaternary compounds of MMg_2FeD_8 (M = Ba, Sr) [29,31] and $Na_2Mg_2NiH_4$ [9], which also contain isolated D^{-} anions. In $[NiH_4]^{4-}$ and $[TH_6]^{4-}$ (T = Fe,

Ru) containing compounds, such as Mg_2FeH_6, these cubes typically assemble in corner sharing three-dimensional arrays [3].

The anionic D^- is enveloped by a distorted octahedral array, consisting of four Na^+ and two Mg^{2+} (Fig. 2c). These octahedra form layers amid the complex hydride layers, via a combination of edge-sharing and face-sharing interactions. The distortion within the D^- containing octahedron arises from two of the four Na−D2 bonds possessing different bond distances of 2.585(6) and 3.215(8) Å, while the two Mg−D2 bond are practically equidistant at 1.911(11) and 1.937(11) Å. The irregular Na−D2 bond distances result in nonlinear Na−D2−Na bond angles of 163.8(5)°, while the Mg−D2−Mg bond angles are 154.7(7)°. The octahedral geometry around D^- is a rare feature, as the coordination of the anionic hydrogen with M^+ and/or M^{2+} within complex transition metal hydrides has previously been determined to be predominately tetrahedral ($Na_2Mg_2NiH_6$ [9], $LaMg_2NiH_7$ [5], $SrMg_2FeH_8$ [29], $BaMg_2FeH_8$ [32], $Ca_4Mg_4FeH_8$ [33], $LaMg_2PdH_7$ [34,35]), linear or trigonal bipyramidal configurations ($LiMg_2RuH_7$, Mg_3MnH_7) [3]. $La_2MgNi_2H_8$, which contains isolated dinuclear $[Ni_2D_7]^{7-}$ and tetranuclear $[Ni_4D_{12}]^{12-}$ complexes, has been determined to coordinate D^- in both tetrahedral and octahedral environments [36]. Complex hydrides containing an octahedral H^- center have been previously observed in the perovskite structures such as $NaMgH_3$ [37].

The crystal structure of $Na_2Mg_2RuD_8$ is identical to that of $Na_2Mg_2FeD_8$, albeit an expansion of the unit cell parameters, with an overall volume expansion of 6.0 % (Fig. 2 and Table 1). This enlargement leads to a concomitant elongation of *T*−D bond distances, which is anticipated due to the increase in atomic radius of the metal center (Ru−D1 = 1.7074(27) Å, Ru−D3 = 1.7488(17) Å). The average Ru−D bond distance of 1.7227(20) Å coincides with other reported

$[RuD_6]^{4-}$ complexes, such as the archetypal Mg_2RuD_6 (1.673(4) Å),[4] Na_4RuD_6 (1.792(9) Å),[38] and the quaternary $BaMg_2RuD_8$ (1.717(2), 1.680(3) Å) [39].

3.3 Vibrational Spectroscopy

FT-IR and Raman spectroscopy studies were conducted on $Na_2Mg_2FeH_8$ and its deuteride analogue, while harmonic frequencies were calculated by DFT methods. Due to the complicated structure of this compound (space group *Pbam*, $Z = 2$), compared to the relatively simple M_2FeH_6 analogues (space group *Fm−3m*, $Z = 4$), the requirement for these complementary spectroscopic techniques to be corroborated by DFT calculations can easily be realized. The Γ-point phonon frequencies obtained by first-principles calculations in the 26-atom unit cell are listed in the Supplementary Information. There are a total of 75 optical Γ-phonon modes belonging to the irreducible representation $11A_g + 8A_u + 7B_{1g} + 12B_{1u} + 7B_{2g} + 12B_{2u} + 11B_{3g} + 7B_{3u}$. The A_g, B_{1g}, B_{2g} and B_{3g} modes are Raman active; B_{1u}, B_{2u}, and B_{3u} modes are IR active; while the A_u mode is inactive in both Raman and FT-IR.

The experimental and DFT results support the crystal structure obtained from the diffraction data; with the observation of the vibrational modes for the $[FeH_6(D_6)]^{4-}$ and isolated $H(D)^-$ anions, the latter of which has not been measured previously for other quaternary complex transition metal hydrides. The FT-IR spectrum of $Na_2Mg_2FeH_8$ (Fig. 3b and Table 3), shows a multiplet of strong vibrational bands between 1752 and 1274 cm^{-1}. With the assistance of the DFT calculated frequencies, the peaks at 1752 and 1645 cm^{-1} are assigned to the octahedral Fe−H stretching vibrations, while the peaks at 1416 and 1274 cm^{-1} are attributed to the vibrational modes of the H^- anions. Fe−H bending vibrations are observed at 856, 783 and 650 cm^{-1}, while the peak at 1575 cm^{-1} is assigned as overtones and combinations of the A_g and B_{3u}

bending modes. The spectrum for $Na_2Mg_2FeH_8$ is in contrast to that of Mg_2FeH_6, which exhibits only three peaks (Figure 3a and Table 3), all of which are attributed to Fe−H stretching, with the strongest being observed at 1843 cm^{-1}. This stretching band arises at a larger wavenumber than that of the most intense Fe−H stretching band of $Na_2Mg_2FeH_8$ (1575 cm^{-1}) due to the increased Fe−H bond distances of $Na_2Mg_2FeH_8$ (Fe−D 1.592(6) Å) compared to Mg_2FeH_6 (Fe−D 1.556(5) Å[25]) [40].

FIGURE 3

Table 3.

The octahedral Fe−H(D) and isolated $H(D)^-$ vibrational modes are also easily distinguished in the Raman spectra of the $Na_2Mg_2FeH_8$ and deuteride analogue. For the hydride analogue (Fig. 3c), peaks at 1874, 1765 and 1732 cm^{-1} are attributed to the Fe−H stretching modes, while one H^- vibrational mode is observed at 1412 cm^{-1}. One Fe−H bending mode is observed at 1076 cm^{-1}. The Raman spectrum for $Na_2Mg_2FeD_8$ (Fig. 3d) is very similar to its hydride counterpart despite the expected isotopic shift of √2. The Fe−D stretching modes are observed at 1338, 1279, 1238 cm^{-1}, and a bending mode at 732 cm^{-1}, while a weak D^- vibration is observed at 1011 cm^{-1}. Four translation modes are observed below 360 cm^{-1} at nearly identical positions for the hydride and deuteride, suggesting that these modes are not ubiquitous to H/D vibrations.

4. Conclusions

The complex transition metal hydrides $Na_2Mg_2TH_8$ (T = Fe, Ru) and their deuteride analogues have been synthesized for the first time and their structures refined by the Rietveld method using SR-PXD and PND data. The compounds are isostructural and crystallize in the orthorhombic space group *Pbam* and represent a new family of group eight metal hydride compounds, which incorporate independently coordinated ionic and covalent hydrogen. $Na_2Mg_2FeH_8$ is the first $[FeH_6]^{4-}$ complex to be stabilized by monovalent Na^+ ions rather than divalent M^{2+} (M = Mg, Ca, Sr, Eu, Yb, Ba) only. As such, the octahedral complex transition metal hydride anion is surrounded by a cubic array of four Mg^{2+} and four Na^+, forming two-dimensional layers.

An intriguing feature of these materials is the distorted octahedral coordination of the isolated H^- anions by four Na^+ and two Mg^{2+}, which forms a combination of edge- and face-sharing layers amid the complex hydride layers.

FT-IR and Raman spectroscopies corroborate the structure of $Na_2Mg_2FeH(D)_8$ by the correlation of experimental and DFT calculated data. For the first time in a quaternary complex transition metal hydride, the determination of the vibrational modes for the H^- anions has been accomplished, as well as the observation of the characteristic Fe−H(D) vibrational modes.

Appendix A. Supplementary material

Tabulated atomic positions for the DFT calculated structures, bond distances and bond angles of $Na_2Mg_2FeD_8$ and $Na_2Mg_2RuD_8$ (experimental and theory); list of peaks corresponding to the unknown phase in $Na_2Mg_2RuD_8$ SR-XRD data; DFT calculated Γ-phonon modes. Supplementary data associated with this article can be found in the online version at …...

Acknowledgements

We would like to thank the project teams at the Swiss Norwegian Beam Line (SNBL) of the European Synchrotron Research Facility (ESRF), Grenoble for their skillful assistance. Financial support from JSPS KAKENHI Grant Number 25220911 and Integrated Project of ICC-IMR at Tohoku University is gratefully acknowledged, as well as the use of SR16000 supercomputing resources at the Center for Computational Materials Science of the Institute for Materials Research, Tohoku University.

References

[1] A. Züttel, M. Hirscher, B. Panella, K. Yvon, S. Orimo, B. Bogdanović, et al., Hydrogen Storage, in: Hydrog. as a Futur. Energy Carr., Wiley-VCH Verlag GmbH & Co. KGaA, 2008: pp. 165–263.

[2] J.J. Reilly, R.H. Wiswall, Inorg. Chem. 7 (1968) 2254–2256.

[3] K. Yvon, Chimia (Aarau). 52 (1998) 613–619.

[4] B. Huang, F. Bonhomme, P. Selvam, K. Yvon, P. Fischer, J. Less Common Met. 171 (1991) 301–311.

[5] G. Renaudin, L. Guenee, K. Yvon, J. Alloys Compd. 350 (2003) 145–150.

[6] M. Matsuo, H. Saitoh, A. Machida, R. Sato, S. Takagi, K. Miwa, et al., RSC Adv. 3 (2013) 1013–1016.

[7] H. Saitoh, S. Takagi, M. Matsuo, Y. Iijima, N. Endo, K. Aoki, et al., APL Mat. 2 (2014) 076103.

[8] K. Kadir, D. Noréus, Inorg. Chem. 46 (2007) 3288–3289.

[9] M. Orlova, J.-P. Rapin, K. Yvon, Inorg. Chem. 48 (2009) 5052–5054.

[10] S. Orimo, Y. Nakamori, J.R. Eliseo, A. Zuttel, C.M. Jensen, Chem. Rev. 107 (2007) 4111–4132.

[11] K. Miwa, S. Takagi, M. Matsuo, S. Orimo, J. Phys. Chem. C. 117 (2013) 8014–8019.

[12] S. Takagi, T.D. Humphries, K. Miwa, S. Orimo, Appl. Phys. Lett. 104 (2014) 203901.

[13] S.F. Parker, Coord. Chem. Rev. 254 (2010) 215–234.

[14] A.P. Hammersley, Fit2D: An introduction and Overview; ESRF Internal Report., 1997.

[15] B.C. Hauback, H. Fjellvåg, O. Steinsvoll, K. Johansson, O.T. Buset, J. Jørgensen, J. Neutron Res. 8 (2000) 215–232.

[16] A. Boultif, D. Louer, J. Appl. Crystallogr. 37 (2004) 724–731.

[17] J. Laugier, B. Bochu, LMGP-Suite Programs Interpret. X-Ray Exp. ENSP/Laboratoire Des Matériaux Du Génie Phys. Saint Martin d'Héres, Fr.

[18] A.C. Larson, R.B. Von Dreele, Los Alamos Natl. Lab. Rep. LAUR. (2000) 86–748.

[19] B.H. Toby, J. Appl. Crystallogr. 34 (2001) 210–213.

[20] P.E. Blöchl, Phys. Rev. B. 50 (1994) 17953–17979.

[21] G. Kresse, D. Joubert, Phys. Rev. B. 59 (1999) 1758–1775.

[22] J.P. Perdew, K. Burke, M. Ernzerhof, Phys. Rev. Lett. 77 (1996) 3865–3868.

[23] G. Kresse, J. Hafner, Phys. Rev. B. 47 (1993) 558–561.

[24] G. Kresse, J. Furthmuller, Phys. Rev. B. 54 (1996) 11169–11186.

[25] J.J. Didisheim, P. Zolliker, K. Yvon, P. Fischer, J. Schefer, M. Gubelmann, et al., Inorg. Chem. 23 (1984) 1953–1957.

[26] P. Zolliker, K. Yvon, P. Fischer, J. Schefer, Inorg. Chem. 24 (1985) 4177–4180.

[27] P. Zolliker, K. Yvon, P. Fischer, J. Schefer, Helv. Chim. Acta. 57 (1984) 754.

[28] C.G. Shull, E.O. Wollan, G.A. Morton, W.L. Davidson, Phys. Rev. 73 (1948) 842–847.

[29] B. Huang, K. Yvon, P. Fischer, J. Alloys Compd. 187 (1992) 227–232.

[30] P. Zolliker, K. Yvon, J.D. Jorgensen, F.J. Rotella, Inorg. Chem. 25 (1986) 3590–3593.

[31] B. Huang, K. Yvon, P. Fischer, J. Alloys Compd. 227 (1995) 121–124.

[32] B. Huang, K. Yvon, P. Fischer, J. Alloys Compd. 204 (1994) 5–8.

[33] B. Huang, K. Yvon, P. Fischer, J. Alloys Compd. 190 (1992) 65–68.

[34] K. Yvon, J.-P. Rapin, N. Penin, Z. Ma, M.Y. Chou, J. Alloys Compd. 446–447 (2007) 34–38.

[35] S.F. Parker, J.W. Taylor, H. Herman, J.-P. Rapin, N. Penin, K. Yvon, J. Alloys Compd. 470 (2009) 80–84.

[36] J.-N. Chotard, Y. Filinchuk, B. Revaz, K. Yvon, Angew. Chemie. 118 (2006) 7934–7937.

[37] E. Rönnebro, D. Noréus, K. Kadir, A. Reiser, B. Bogdanović, J. Alloys Compd. 299 (2000) 101–106.

[38] M. Kritikos, D. Nore´us, A.F. Andresen, P. Fischer, J. Solid State Chem. 92 (1991) 514–519.

[39] B. Huang, F. Gingl, F. Fauth, A. Hewat, K. Yvon, J. Alloys Compd. 248 (1997) 13–17.

[40] H. Hagemann, V. D'Anna, L.M. Lawson Daku, S. Gomes, G. Renaudin, K. Yvon, J. Phys. Chem. Solids. 72 (2011) 286–289.

Figures and Table caption

Fig. 1. Rietveld refinement plot of (a) SR-XRD and (b) PND data for $Na_2Mg_2FeD_8$ and (c) SR-XRD and (d) PND data for $Na_2Mg_2RuD_8$. Experimental data as red circles, calculated diffraction pattern as black line and the difference plot in blue. Tick marks show positions for: (a) and (b) $Na_2Mg_2FeD_8$ (bottom), Fe, Mg_2FeD_6 and NaD (top), respectively; (c) and (d) $Na_2Mg_2RuD_8$ (bottom), Ru and unknown phase (top), respectively. The profile of the unknown phase in $Na_2Mg_2RuD_8$ was by the Le Bail method. $\lambda = 0.70135$ Å (SR-XRD) and 1.5548 Å (PND).

Fig. 2. Structural representations of $Na_2Mg_2TD_8$ (T = Fe, Ru). (a) Extended structure viewed along the *a* axis (thick, gray lines outline the unit cell); (b) coordination of $[TD_6]^{4-}$ octahedron; (c) coordination of D^- (D2); and (d) interaction between $[TD_6]^{4-}$ containing cubes (D^- atoms

omitted for clarity). Green spheres represent *T* (Fe or Ru); turquoise spheres are Na; orange spheres are Mg; small blue spheres are octahedral D atoms; large blue spheres are D^-.

Fig. 3. (a) FT-IR spectrum of Mg_2FeH_6, (b) FT-IR and (c) Raman spectra of $Na_2Mg_2FeH_8$ and Raman spectrum (d) of $Na_2Mg_2FeD_8$. Numbered vibrations correlate to those in Table 3. Only the strongest Fe−H vibration for Mg_2FeH_6 has been labelled.

Table 1. Crystallographic data for $Na_2Mg_2FeD_8$ and $Na_2Mg_2RuD_8$ at room temperature obtained by combined Rietveld refinement with SR-PXD and PND data. Estimated standard deviations are given in parenthesis.

Table 2. Selected interatomic bond distances (Å) and selected angles (°) at room temperature for $Na_2Mg_2TD_8$ (*T* = Fe, Ru) obtained from combined Rietveld refinement of SR-PXD and PND data. Estimated standard deviations are given in parenthesis.

Table 3. Observed and calculated FT-IR and Raman vibrations for $Na_2Mg_2FeH(D)_8$ and Mg_2FeH_6 (cm^{-1}).

Table 1

Phase Data					
Chemical formula		$Fe\ Mg_2\ Na_2\ D_8$		$Ru\ Mg_2\ Na_2\ D_8$	
M_r		166.55		211.77	
Crystal system		Orthorhombic		Orthorhombic	
Space group		*Pbam* (55)		*Pbam* (55)	
Cell parameters (Å)		a = 5.30527(8)		a = 5.37969(5)	
		b = 11.03743(16)		b = 11.11847(10)	
		c = 4.47783(6)		c = 4.64792(4)	
Cell volume (Å^3)		262.206(5)		278.010(3)	
Z		2		2	
wR		0.079		0.056	
χ^2		11.34		9.32	
Atom	**Wyckoff position**	***x/a***	***y/b***	***z/c***	U_{iso} (Å^2)
Fe1	2*a*	0.0	0.0	0.0	0.0022(4)
Mg1	4*h*	0.0291(4)	0.12968(11)	0.5	0.0022(4)
Na1	4*g*	0.0071(5)	0.35998(12)	0.0	0.0100(5)
D1	4*g*	0.0390(19)	0.1447(8)	0.0	0.0213(12)
D2	4*h*	0.3371(20)	0.2238(11)	0.5	0.0309(27)
D3	8*i*	0.2907(10)	0.4906(7)	0.2537(15)	= U_{iso}(D1)
Ru1	2*a*	0.0	0.0	0.0	0.00074(7)
Mg1	4*h*	0.03664(23)	0.13163(9)	0.5	0.00261(20)
Na1	4*g*	−0.0028(5)	0.35871(8)	0.0	0.00647(32)
D1	4*g*	0.02959(33)	0.15290(24)	0.0	0.02223(12)
D2	4*h*	0.35300(27)	0.2258(4)	0.5	0.0261(6)
D3	8*i*	0.27263(23)	0.49517(26)	0.2795(5)	= U_{iso}(D1)

Table 2

		$Na_2Mg_2FeD_8$	$Na_2Mg_2RuD_8$
Atom 1	**Atom 2**	***d* (Å)**	***d* (Å)**
T	D1	1.610(9)	1.7074(27)
	D3	1.592(6)	1.7488(17)
	Mg	2.6618(7)	2.7534(5)
	Na	3.0373(26)	3.1018(25)
Mg	D1	2.2457(7)	2.33672(23)
	D2	1.911(11)	1.868(5)
	D2	1.937(11)	1.9983(34)
	D3	2.118(7)	2.0729(29)
	D3	2.139(7)	2.2147(23)
Na	D1	2.382(9)	2.2950(26)
	D1	2.484(10)	2.519(4)
	D1	2.822(10)	2.867(4)
	D2	2.585(6)	2.6240(12)
	D2	3.215(8)	3.3328(27)
	D3	2.373(7)	2.5196(24)
	D3	2.551(7)	2.5676(21)
Atoms		**Angle (°)**	**Angle (°)**
D3−*T*−D3		180.0	180.0
D3−*T*−D3		88.9(4)	84.04(14)
D1−*T*−D3		88.6(4)	88.18(9)
D1−*T*−D1		180.0	180.0
T−D1−Na		168.5(6)	170.29(16)
Mg−D2−Mg		154.7(7)	153.54(15)
Na−D2−Na		163.8(5)	160.1(9)

Table 3

	$MgFeH_6$	$Na_2Mg_2FeH(D)_6$					Assignment
	IR	IR		Raman			
	H	H	H (DFT)	H	H (DFT)	D	
1	1786 vs						υ(Fe−H) (T_{1u})
2				1874 s	1808	1338 s	υ(Fe−H) (A_g/B_{3g})
3				1756 m	1753	1279 m	υ(Fe−H) (B_{1g}/B_{2g})
4		1752 s	1727				υ(Fe−H) (B_{1u}/B_{2u})
5				1732 m	1744	1238 m	υ(Fe−H) (A_g)
6		1645 s br	1627				υ(Fe−H/D) (B_{3u})
7		1575 vs					δ(Fe−H) (A_g) + δ(Fe−H) (B_{2u})
8		1416 s	1360				(H^-/D^-) (B_{1u})
9				1412 w	1431	1011 w	(H^-/D^-) (B_{3g})
10		1274 s	1229				(H^-/D^-) (B_{2u})
11				1076 vw	1018	732	δ(Fe−H/D) (A_g)
12		856 w	820				δ(Fe−H) (B_{2u})
13		783 m	782				δ(Fe−H) (B_{3u})
14		650 m	637				δ(Fe−H) (B_{3u})
15		444 m	458				libration/translation (B_{2u})
16				345 w	346	360 w	translation (A_g)
17				261 m	303	262 m	translation (B_{3g})
18				246 m	236	247 m	translation (B_{3g})
19				229 m	223	230 m	translation (B_{2g})

υ= stretching vibration; δ bending vibration; s = strong; m = medium; w = weak; v = very; br = broad.

Figure 1

Click here to download high resolution image

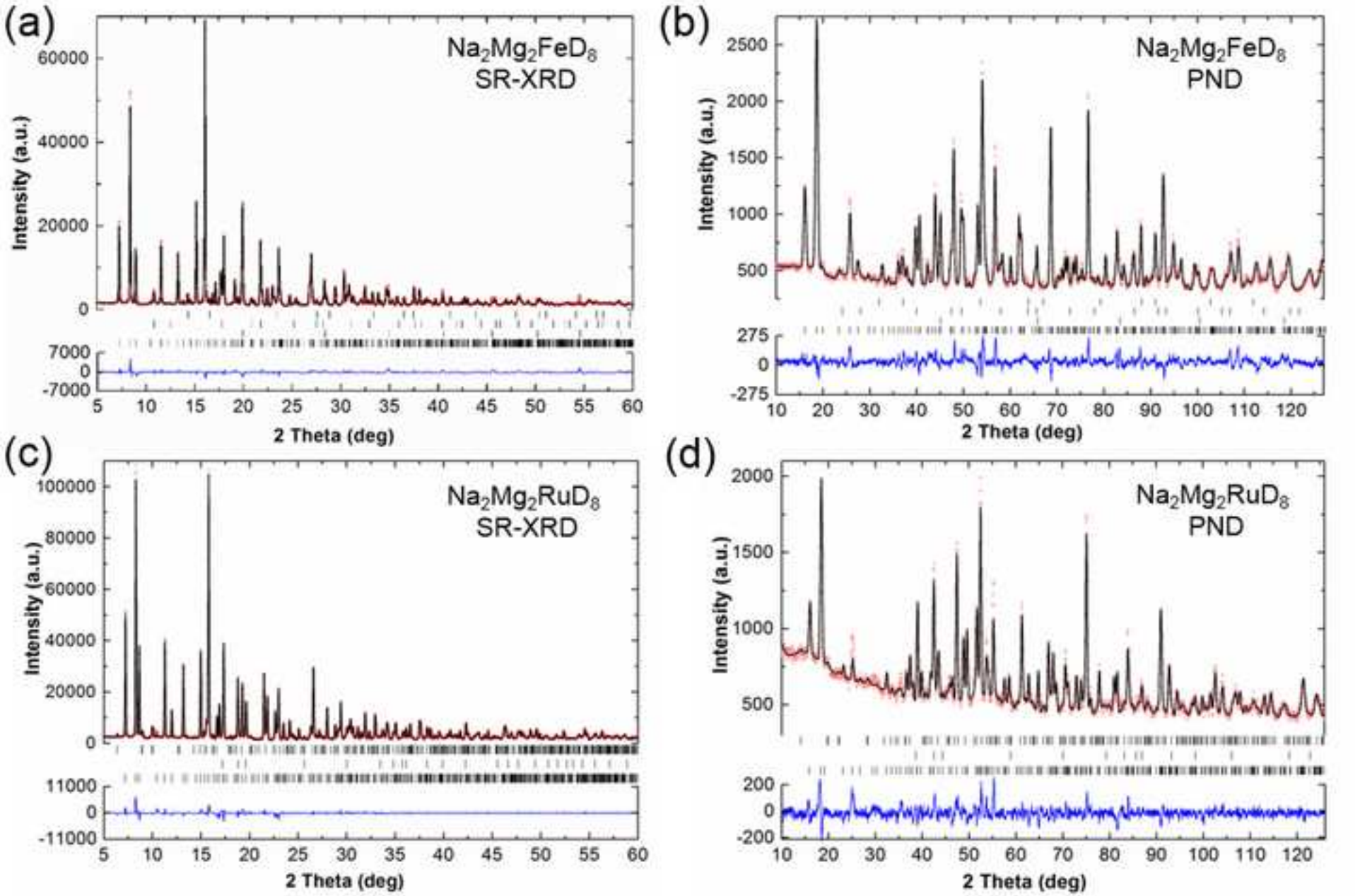

Figure 2

Click here to download high resolution image

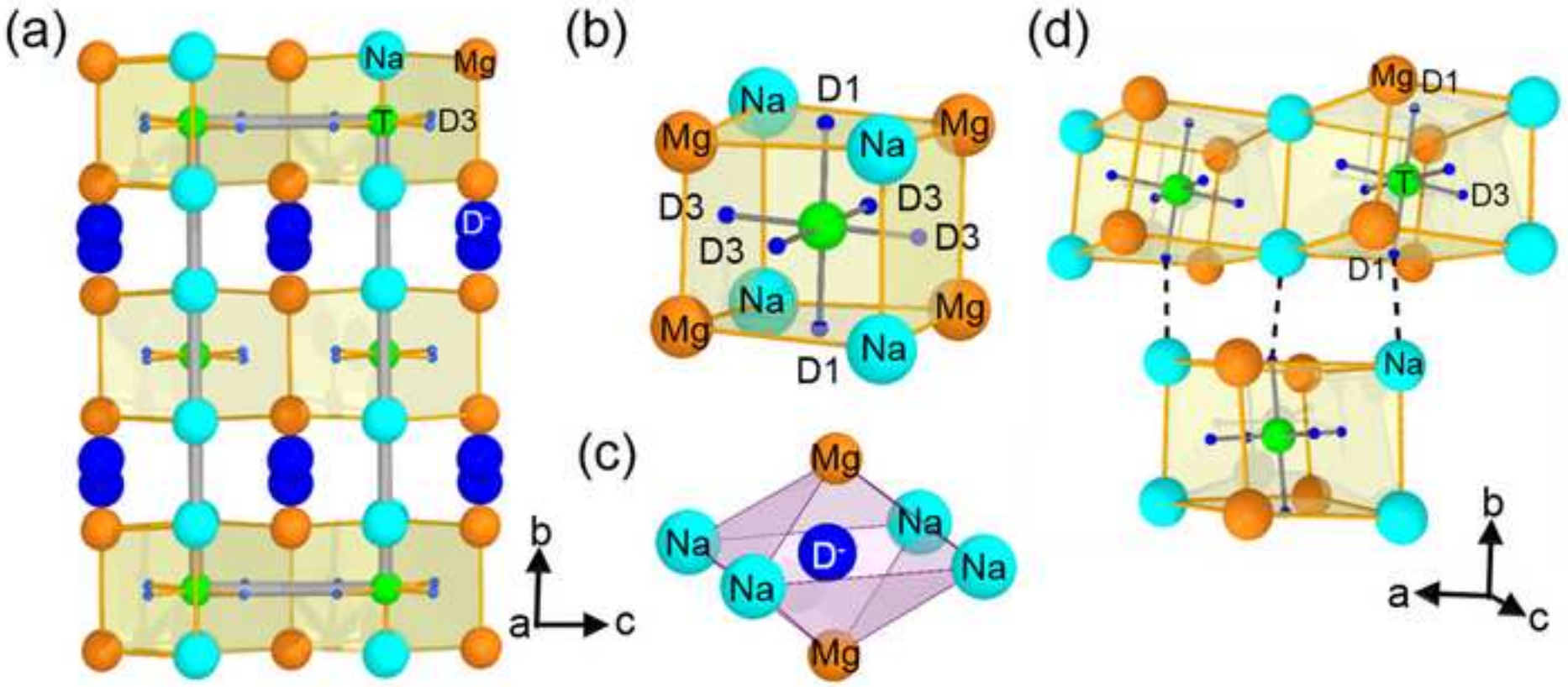

Figure 3

Click here to download high resolution image